



OPEN Anti-angiogenic effects of cationic zinc (II) phthalocyanine derivatives through photodynamic therapy

Seyma Isik^{1,2}, Mukaddes Ozcesmeci³, Ayfer Kalkan Burat³, Esin Hamuryudan³, Ozge Can⁴✉ & Muge Serhatli¹✉

In this study, the *in vitro* photodynamic therapy (PDT) activity of two zinc phthalocyanines (ZnPc1 and ZnPc2) was systematically examined in human umbilical vein endothelial cells, focusing on PDT-induced cytotoxicity, reactive oxygen species (ROS) generation, and inhibition of angiogenic processes. Both the ZnPcs demonstrated minimal cytotoxicity in the absence of light, confirming their safety as photosensitizers. ZnPc-PDT led to significant cell death via apoptosis. ZnPc1 exhibited enhanced ROS generation, particularly at elevated concentrations. Furthermore, ZnPc1-mediated PDT showed more pronounced inhibition of endothelial cell migration, invasion, and capillary-like tube formation than ZnPc2. Wound-healing assays revealed a substantial delay in human umbilical vein endothelial cell (HUVEC) migration following ZnPc1-PDT, which also displayed a more significant inhibition of VEGF-induced directional migration and invasion. Endothelial tube formation was more effectively disrupted by ZnPc1-PDT, even at lower concentrations, compared to ZnPc2. Collectively, these findings highlight the superior cytotoxic and anti-angiogenic properties of ZnPc1 compared with ZnPc2, highlighting its potential as a highly effective photosensitizer for photodynamic therapy. The ability of ZnPc1 to simultaneously target tumor cells and disrupt angiogenesis establishes it as a potent candidate for integrated cancer therapies that combine both antitumor and antiangiogenic strategies, offering a more effective approach to combat cancer progression.

Keywords Angiogenesis, Photodynamic therapy, Phthalocyanine, Migration, Invasion

Angiogenesis, the formation of new blood vessels from pre-existing ones, plays a crucial role in tumor growth and metastasis by delivering oxygen and nutrients to rapidly dividing tumor cells¹. Targeting angiogenesis is a key strategy in cancer treatment, as it disrupts the blood supply necessary for tumor growth and metastasis, making it a highly effective therapeutic approach for limiting cancer progression². Photodynamic therapy (PDT) is a highly effective treatment that employs photosensitizers (PS), light, and molecular oxygen to generate reactive oxygen species (ROS), targeting and destroying tumor cells without damaging the surrounding healthy tissue³. In recent years, the ability of PDT to not only destroy tumor cells but also impair tumor vasculature, specifically by inhibiting angiogenesis, has attracted significant attention^{4–9}. Szafraniec et al. reported that PDT effectively induces apoptosis in endothelial cells. Their findings further demonstrated that, compared to tumor cells, endothelial cells were significantly more sensitive to photodynamic therapy, highlighting their enhanced efficacy against the vascular component of tumors⁴. Suzuki et al. reported the vascular shutdown effect of PDT, showing that PDT effectively induced cell death and resulted in disintegration of endothelial tube structures *in vitro*⁵. It has also been shown to exhibit a pronounced inhibitory effect on endothelial cell migration, metalloproteinase activity, and tube formation, demonstrating potent disruption of key processes involved in angiogenesis⁶.

Chemically and photochemically robust phthalocyanines (Pcs) have large extinction coefficients and favorable quantum yields. In addition, the absorption and fluorescence maxima in the presence of appropriate substituents and the central metal (Zn, Al, or Ga) can be easily modified^{10,11}. Thus, Pcs are advanced second-generation photosensitizers, known for their strong absorption in the 650–850 nm region, which allows for deeper tissue penetration during photodynamic therapy, improving the effectiveness of the treatment¹². Phthalocyanin-

¹TUBITAK Marmara Research Center, Climate Change and Life Sciences, Biotechnology Research Group, 41470 Kocaeli, Turkey. ²Department of Medical Biotechnology, Graduate School of Health Sciences, Acibadem Mehmet Ali Aydinlar University, 34752 Istanbul, Turkey. ³Department of Chemistry, Istanbul Technical University, 34469 Istanbul, Turkey. ⁴Department of Biomedical Engineering, Faculty of Engineering and Natural Sciences, Acibadem Mehmet Ali Aydinlar University, 34752 Istanbul, Turkey. ✉email: ozge.can@acibadem.edu.tr; muge.serhatli@tubitak.gov.tr

mediated photodynamic therapy has shown significant potential for inducing both apoptosis and necrosis through the generation of reactive oxygen species (ROS)^{13–15}. Moreover, recent studies have highlighted the significant potential of phthalocyanine molecules in targeting angiogenesis by interfering with key processes, such as endothelial cell migration, invasion, and tube formation, thereby effectively inhibiting fundamental pathways crucial for vascularization^{16,17}. Zinc phthalocyanines, in particular, show intense fluorescence in the near-IR region; therefore, they are of interest in materials science and biomedical fields. ZnPcs can be used against bacteria owing to their optical sensitivity, and can also be used for cancer treatment in PDT^{18,19}. Schmidt et al. (2018) investigated the anti-angiogenic effects of zinc phthalocyanine-mediated photodynamic therapy (ZnPc-PDT) using a chorioallantoic membrane (CAM) assay. Their research revealed that ZnPc-PDT significantly reduced angiogenic sprouting, increased the number of non-perfused areas, and induced substantial degeneration of the vascular network in CAM¹⁶. Kuzyniak et al. also reported that ZnPc-PDT induced significant degradation of blood vessels and the complex capillary network within CAM, thereby highlighting the anti-angiogenic properties of Pc-based photosensitizers¹⁷. In this study, we report the *in vitro* photodynamic therapy activities of peripheral and non-peripheral tetra-substituted cationic zinc phthalocyanines (ZnPc1 and ZnPc2) in HUVECs. Specifically, we underscore the comparative analysis of two distinct zinc phthalocyanines (ZnPc1 and ZnPc2) in terms of their photophysical properties, cytotoxicity, and anti-angiogenic effects which represents a systematic evaluation that has not been previously reported. Furthermore, our study uniquely investigates the differential impacts of these derivatives on endothelial cells, providing valuable insights into the development of photosensitizers with enhanced therapeutic potential for photodynamic therapy. PDT-induced cytotoxicity, generation of reactive oxygen species, and the underlying mechanisms of cell death were investigated. Moreover, the inhibitory effects of ZnPc-PDT on key endothelial cell functions essential for angiogenesis, including wound healing, directed cell migration, invasion, and capillary-like tube formation were examined. In our previous study, we demonstrated the effectiveness of PDT using ZnPc molecules in various cancer cell lines (data not shown). ZnPc-PDT exhibited a remarkable capacity to induce targeted cytotoxicity in tumor cells and inhibit processes critical for angiogenesis. These findings collectively underline the substantial potential of ZnPcs as photosensitizers in PDT for effective anti-angiogenic therapy, capable of both direct tumor destruction and disruption of the vascular supply essential for tumor growth and metastasis.

Methods

Materials

Human umbilical vein endothelial cells (HUVECs), endothelial basal media EBM-2, and EGM-2 SingleQuots were purchased from Lonza (Switzerland). Penicillin–streptomycin and Hank's Balanced Salt Solution (HBSS) were purchased from Thermo Fisher Scientific (United States). The apoptosis/necrosis Detection Kit and Calcein AM were purchased from Abcam (Cambridge, UK). The cell proliferation reagents WST-1 and 2',7'-dichlorofluorescein diacetate (DCFDA) were purchased from Sigma Aldrich (United States). Matrigel Matrix, BioCoat Angiogenesis System, FluoroBlok 24 Multiwell Insert Plates with a 3.0 were purchased from Corning (United States).

Cell culture

HUVECs were cultured in endothelial basal media (EBM-2) supplemented with 1% penicillin (10,000 Units/ml) - streptomycin (10,000 Units/ml), and EGM-2 SingleQuots containing growth factors (insulin-like growth factor, human fibroblast growth factor, human epidermal growth factor, vascular endothelial growth factor) and ascorbic acid, heparin, hydrocortisone, and 2% fetal bovine serum (FBS). The cells were passaged three times per week, considering their population doubling times. Mycoplasma tests were conducted monthly on the cell lines using a Lucetta 2 Luminometer and MycoAlert Plus Mycoplasma Detection Kit.

Photodynamic therapy

HUVECs were seeded into 96-well plates (5×10^3 cells/well) and incubated in a humidified incubator (37 °C, 5% CO₂) for 24 h. ZnPc molecules (1–10 μM) were administered to the cells and further incubated for 1 h to facilitate cellular uptake. Photodynamic therapy (PDT) was applied using CETONI LED equipment (Germany), delivering 20 joules cm⁻² at the appropriate wavelength (650–670 nm), based on the absorption characteristics of the ZnPc molecules.

Cytotoxicity assay

Cell viability was assessed 24 h post-treatment using a colorimetric WST-1 assay. The culture medium was replaced with WST-1 solution (1:10, in complete media) and incubated at 37 °C for 3 h. Absorbance values were recorded at 450 and 650 nm using a Cytation 5 multi-plate reader. Percentage viability was calculated relative to the untreated controls. The concentration range of ZnPc molecules for PDT was determined based on the dark cytotoxicity results.

Oxidative stress evaluation

Following PDT, intracellular ROS levels were measured at 30 min and 24 h using 2',7'-dichlorofluorescein diacetate (DCFDA). The culture medium was replaced with DCFDA (10 μM in HBSS), and the cells were incubated at 37 °C for 30 min. Fluorescence intensity (ex/em: 504/529 nm) was recorded using a Cytation 5 multi-plate reader (Agilent, United States). As a control, 50 μM H₂O₂ was used as a control. The percentage ROS levels were calculated relative to the untreated control.

Cellular death mechanism

The mechanism of cell death was evaluated 24 h after photodynamic therapy using an Apoptosis/Necrosis Detection Kit following the manufacturer's instructions. Briefly, after PDT, the cells were stained with the following fluorescent dyes: Apopxin for apoptotic cells, 7-AAD for necrotic cells, and CytoCalcein for live cells, followed by incubation for 60 min. Images were taken using the Cytation 5 device (Agilent, United States), and the number of apoptotic, necrotic, or live cells was quantified using Gen5 software.

Wound healing assay

Spontaneous cell migration was assessed using a wound healing assay. Cells were seeded in 96-well plates (1×10^4 cells/well) and incubated in a humidified incubator (37 °C, 5% CO₂) to create a confluent monolayer. Then, complete medium was changed with starvation medium (EBM-2 supplemented with 0.5% FBS), and incubated for 18 h to arrest cells in the G₀ phase of the cell cycle. Wounds of equal size were created on the cell monolayers using Autostrach equipment. ZnPc molecules (1–10 μM) were administered and PDT was applied to the cells. The plate was then placed in a Cytation 5 device (5% CO₂, 37 °C), and cellular migration toward the wound area was imaged for 24 h. The wound areas were analyzed using the Gen5 software, and the results were expressed as the percentage of empty wound areas relative to the control. As control groups, untreated cells (w/o), cells treated with ZnPc alone without PDT (dark) were used.

Directional migration assay

Directional cell migration was evaluated using the xCELLigence MP real-time cell analysis system (Agilent, United States)²⁰. The assay was conducted in CIM Plate-16, which functions as a modified Boyden chamber. To enhance cell attachment, the membrane of the upper chamber was coated with 0.1% gelatin and cells (3×10^5 cells/well) were seeded into the upper chamber. ZnPc molecules (1–10 μM, in starvation medium) were then administered, and PDT was applied to the cells. The CIM-16 plate was placed in the xCELLigence device, and impedance-based measurements were recorded every 15 min over a 24-h period to monitor migration in real-time. As control groups, untreated cells (w/o), with or without chemoattractant (VEGF), and cells treated with ZnPc alone without PDT (dark) were used.

Transwell migration and invasion assay

Directional cell migration and invasion were assessed using the transwell assay²¹. The BioCoat Angiogenesis System, FluoroBlok 24 Multiwell Insert Plates with a 3 μm pore size PET membrane, pre-coated with human fibronectin, was utilized to evaluate cell migration. For the invasion assay, PET membranes were uniformly coated with Matrigel matrix. Cells were seeded (3×10^5 cells/mL) into the insert plates, ZnPc molecules (1–10 μM, in starvation medium) were administered, and PDT was applied to the cells. A VEGF-containing starvation medium was added to the lower chamber as a chemoattractant. After 24 h of incubation, the cells were labeled with Calcein AM, and images were taken using the Cytation 5 device. The number of migrated and invaded cells was quantified and analyzed using the Gen5 software. As control groups, untreated cells (w/o), with or without chemoattractant (VEGF) was used.

Tube formation assay

Tube formation assay was performed on 96-well plates pre-coated with 50 μL of Matrigel²². Cells were seeded (2×10^4 cells/mL) in Matrigel-coated wells, ZnPc molecules (1–10 μM) were then administered, and PDT was applied to the cells. Following PDT, tube formation was monitored at 2, 5, 24, and 48 h using a Cytation 5 device. Tubes are defined as networks of cells with junctions connecting them, mimicking capillary-like structures. As control groups, untreated cells (w/o), cells treated with ZnPc alone without PDT (dark) were used.

Statistics

Data are expressed as the mean ± SD. Comparisons between groups were performed using a two-way ANOVA with post hoc test. GraphPad Software (RRID: SCR_002798) was used for statistical analysis. Results are shown as means ± SD of three independent experiments. Statistical significance was set at $p < 0.05$.

Results

Cationic phthalocyanines, ZnPc1 and ZnPc2 (Fig. 1a, b) were synthesized according to the literature^{19,23} and their structures were elucidated by widely used spectroscopic measurements (¹H NMR, FT-IR, and UV-Vis). The results confirmed the structure of the Pcs. When the IR spectra of ZnPc1 and ZnPc2 were compared, aromatic, aliphatic, and etheric CH stretches were detected at 3010–3021, 2924–2849, and 1225–1235 cm⁻¹ for both Pcs. In the ¹H NMR spectra of both Pc compounds, 12 aromatic protons were detected in the range of approximately 9.16–7.81 ppm, while OCH₂ and NH₂ protons appeared at 5.10, 4.21 ppm and 5.33, 4.44 ppm for ZnPc1 and ZnPc2, respectively. NCH₃ protons were detected in very close proximity at 3.49 ppm (for ZnPc1) and 3.55 ppm (for ZnPc2). As expected, cationic phthalocyanines, which are insoluble in common organic solvents, are soluble in water and DMSO. The characteristic B and Q band absorptions were determined from the UV-Vis spectra of ZnPcs in both water and DMSO. As seen in Fig. 1c, the nature of the solvent and the position of the substituents affected the aggregation behavior of Pc molecules. In the absorption spectra of ZnPc1 and ZnPc2 in DMSO, B bands were observed at approximately 340 nm, whereas Q bands were observed at 682 and 704 nm, respectively. Unlike DMSO, water produced double Q bands, which are due to aggregation, at 636 and 670 nm (for ZnPc1) and 653 and 694 nm (for ZnPc2), respectively. When the UV-Vis spectra of ZnPc taken in DMSO and water were compared, it was observed that the Q bands were narrower and sharper, and their absorbance was higher in DMSO, which may be due to the high polar character of water used as the solvent.

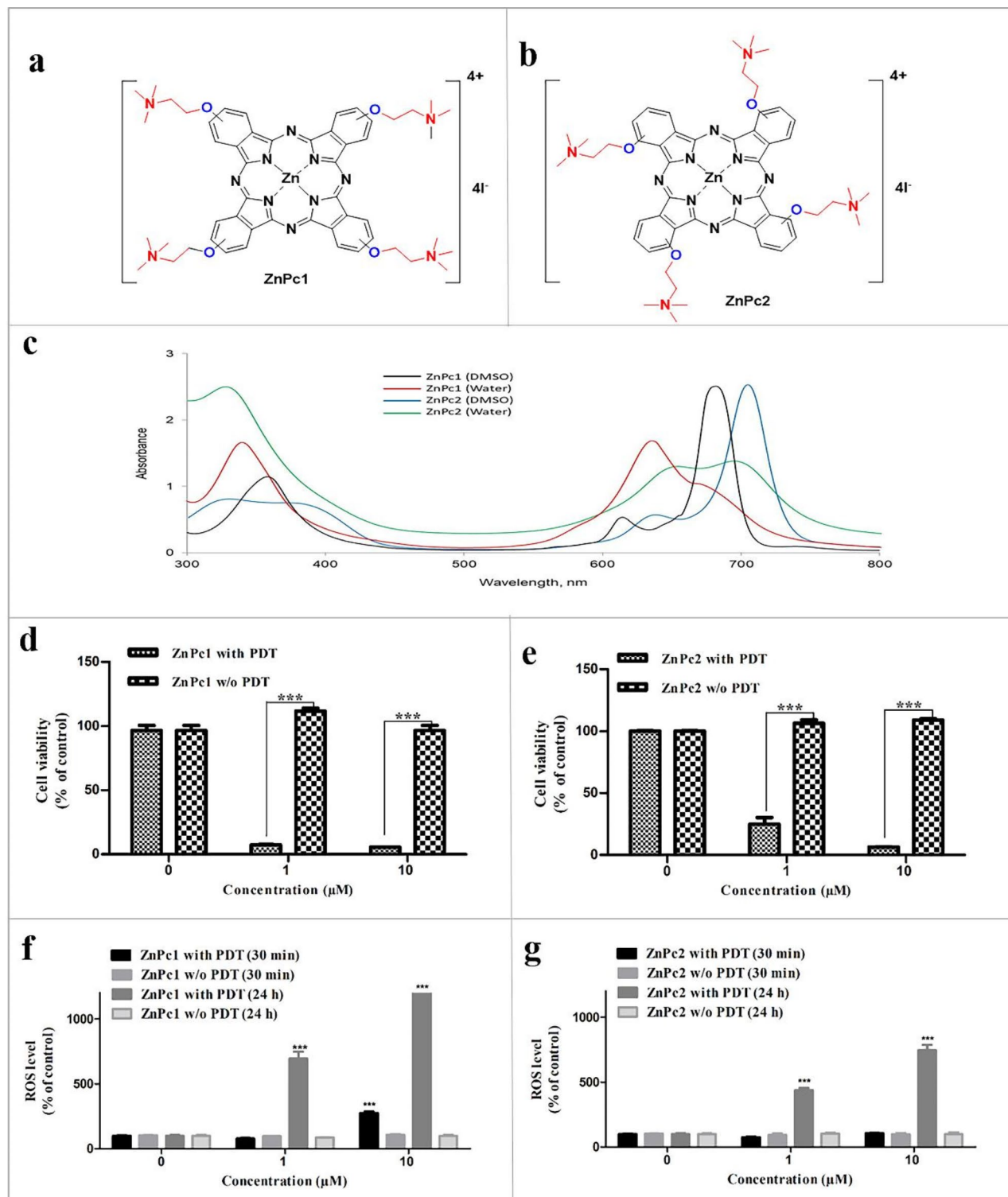


Fig. 1. Chemical structures of (a) peripheral (ZnPc1) and (b) non-peripheral (ZnPc2) tetra-substituted cationic zinc phthalocyanines. (c) UV-Vis absorption spectra of ZnPc1 and ZnPc2 in DMSO and water (5×10^{-5} M). (d, e) Dark and PDT-induced cytotoxicity of ZnPcs on HUVECs. (f, g) PDT-induced ROS production in HUVEC. (d) PDT with ZnPc1 induced significant cytotoxicity, without affecting cell viability in the absence of light in HUVECs. In contrast, (e) PDT with the ZnPc2 molecule caused a dose-dependent cytotoxicity, without affecting cell viability in the absence of light. PDT light dose: 20 joules. cm^{-2} . Results are shown as means \pm SD of three independent experiments. * $p < 0.05$, ** $p < 0.01$ and *** $p < 0.001$. PDT light dose: 20 joules. cm^{-2} . Results are means \pm SD of three independent experiments. * $p < 0.05$, ** $p < 0.01$ and *** $p < 0.001$. PDT light dose: 20 joules. cm^{-2} .

A cell viability assay was conducted to evaluate the cytotoxic effects of ZnPc on HUVECs. The results demonstrated that both ZnPc1 and ZnPc2 at concentrations up to 10 μM exhibited no significant toxicity to HUVECs in the absence of light (Fig. 1d, e). Following PDT, cell viability was significantly decreased with ZnPc1, showing viabilities of 7.2 ± 0.4 and $5.4 \pm 0.2\%$ at concentrations of 1 and 10 μM , respectively, compared to the control group without PDT (Fig. 1d). Similarly, ZnPc2-PDT induced significant cytotoxic effects on HUVECs, particularly at a higher concentration (10 μM), where viability was reduced to $6.5 \pm 0.2\%$, in contrast to $22.5 \pm 5.5\%$ at 1 μM (Fig. 1e). Unlike ZnPc1, ZnPc2-induced cytotoxicity increased in a dose-dependent manner, with the highest concentration resulting in the most substantial cell death.

The intracellular ROS levels were measured to evaluate the extent of PDT-induced oxidative stress (Fig. 1f, g). The results indicated a significant increase in ROS production following PDT, with the most pronounced levels observed 24 h (delayed) post-treatment. Notably, at a 10 μM ZnPc1 concentration, delayed ROS production post-PDT exhibited a remarkable elevation, reaching $1208.9 \pm 54.8\%$ of the control, compared to $692.7 \pm 53.2\%$ at 1 μM (Fig. 1f). A similar pattern was observed with ZnPc2-PDT, where delayed ROS production was significantly higher compared to the control group, reaching 436.1 ± 17.7 and $744.5 \pm 42.9\%$ at 1 and 10 μM concentrations, respectively, showing a dose dependent response (Fig. 1g). Moreover, ZnPc1-PDT exhibited a higher level of delayed ROS production than ZnPc2, and only PDT with 10 μM ZnPc1 resulted in a significant increase in immediate (30 min post-PDT) ROS production.

The mechanism of cell death induced by ZnPc-PDT in HUVECs was investigated (Fig. 2), and the results indicated that ZnPc1-PDT induced significant cell death predominantly through apoptosis at a concentration of 1 μM , with $98.3 \pm 3.5\%$ of cells undergoing apoptosis and only $1.3 \pm 0.9\%$ exhibiting necrosis. However, increasing the ZnPc1 concentration to 10 μM caused a marked shift, with the proportion of apoptotic cells decreasing to $44.3 \pm 0.8\%$, while necrotic cells increased significantly to $55.6 \pm 0.4\%$ (Fig. 2a, c). In contrast, ZnPc2-PDT induced apoptosis at both the concentrations. At 1 μM ZnPc2, $62.6 \pm 1.7\%$ of the cells were apoptotic, whereas necrotic cells accounted for only $0.3 \pm 0.1\%$, and $37.2 \pm 3.4\%$ remained viable. At 10 μM ZnPc2, the proportion of apoptotic cells increased to $97.9 \pm 1.3\%$, with necrosis remaining negligible at $0.3 \pm 0.1\%$ (Fig. 2b, d).

The effect of ZnPc-PDT on spontaneous cell migration was assessed using a wound-healing assay (Figs. 3 and 4). The results indicated that PDT treatment with both ZnPc variants significantly reduced the wound healing capacity of HUVECs in a dose-dependent manner. ZnPc-PDT notably delayed wound closure, whereas even at high concentrations without PDT, ZnPcs did not cause a significant delay compared to the untreated control. Higher concentrations of ZnPcs led to complete inhibition of HUVEC migration toward the wound area following PDT. Wound closure at 24 h post-PDT with lower doses of ZnPc1 and ZnPc2 was $36.5 \pm 2.1\%$ and $64.7 \pm 1.5\%$, respectively.

The effects of ZnPc on directional cell migration and invasion toward VEGF as a chemoattractant were assessed. Migration across the Transwell membrane toward VEGF-containing medium was evaluated over 24 h using both image-based (Fig. 5) and impedance-based real-time (Fig. 6) assays. In the no chemoattractant groups, the percentages of cells that migrated and invaded were 52.3% and 44.3%, respectively. At high concentrations, ZnPc1 induced significant inhibition of migration with no detectable cells, whereas ZnPc2 showed 32.7% migration relative to the control (Fig. 5). Conversely, at low ZnPc concentrations, PDT only moderately affected the HUVEC migration. As with lower concentrations, ZnPc1 showed slightly stronger inhibition than ZnPc2, with identified cell percentages of 74.1% for ZnPc1 and 86.6% for ZnPc2. The results of the invasion assay (Fig. 7) followed a pattern similar to that of the migration assay. To evaluate whether the inhibition of HUVEC migration was time-dependent, the xCELLigence RTCA DP system, a quantitative platform for real-time monitoring, was used (Fig. 6). Significant reductions in HUVEC migration were observed with both ZnPc1 and ZnPc2 in a time- and dose-dependent manner compared with control cells.

The effect of ZnPc on HUVEC tube formation was evaluated using an Endothelial Tube Formation Assay (Fig. 8). The control group developed extensive networks of organized interconnected tubes with complete lumen structures, indicative of typical endothelial tube formation. Similarly, ZnPc without PDT did not impair tube formation, as evidenced by the intact lumen structures, particularly at lower concentrations. However, at higher doses of ZnPc1, the tube structures became highly disorganized and incomplete, and were characterized by fragmented tubes and fewer connections. In contrast to the control, ZnPc-PDT treatment significantly reduced the total tube length and number of tubes, branches, and nodes. At high concentrations, both ZnPcs strongly inhibited endothelial reorganization into tube-like networks, even at the early stages, resulting in isolated round cells or small clusters. At low concentrations of ZnPc1, PDT still exerted an inhibitory effect, leading to disruption of the tube-like networks, which appeared to be fragmented. In contrast, ZnPc2 at low concentrations still formed organized and interconnected tubular structures, although with fewer branches and less organization compared to the controls.

Discussion

In this study, the photophysical properties and therapeutic potential of two ZnPc derivatives, ZnPc1 and ZnPc2, were explored in the context of PDT. Both immediate and prolonged ROS generation were examined, along with evaluations of their effects on cell viability, migration, and invasion, providing insights into the mechanisms by which ZnPc1 and ZnPc2 exert anti-angiogenic effects. A comparative analysis of ZnPc1 and ZnPc2 highlighted distinct behaviors in terms of phototoxicity and anti-angiogenic activity, offering insights into their suitability for PDT applications, particularly for targeting angiogenesis-dependent tumor growth. The findings indicated that solvents significantly affected the electronic properties of the ZnPcs, impacting their effectiveness in generating reactive oxygen species and inducing cytotoxicity in target cells. This solvent sensitivity suggests that a tunable solvent environment could optimize the photophysical features of these compounds, potentially enhancing their effect in PDT applications.

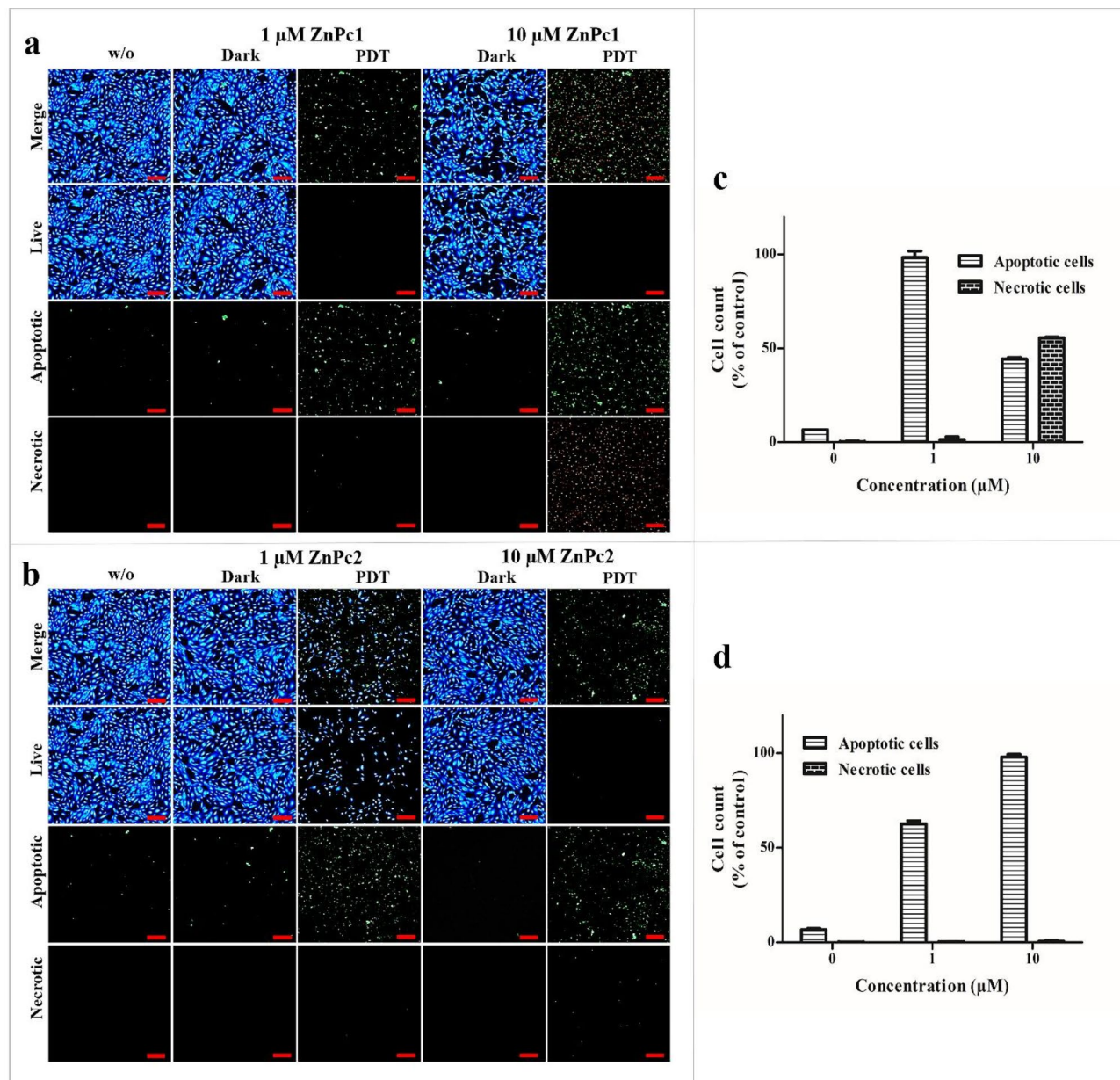


Fig. 2. PDT-induced cellular death mechanism on HUVECs mediated by (a, c) ZnPc1 and (b, d) ZnPc2 molecules. Fluorescence images indicated that HUVECs exhibited both apoptosis and necrosis only with ZnPc1-PDT at high dose, and predominant mechanism with both doses of the molecules was apoptosis (c, d). Apoptotic cells (Apopxin Green dye, green), living cells (Cyto Calcein Violet 450, blue) and necrotic cells (7-AAD, red). Scale bar: 200 μm .

A key characteristic of effective photosensitizers is their low cytotoxicity in the absence of light. The findings confirm the non-toxic nature of the ZnPcs under dark conditions, which is crucial for safe and effective photosensitizers in PDT. Upon activation with light, both ZnPc1 and ZnPc2 significantly reduced cell viability in HUVECs, with cytotoxicity increasing in a dose-dependent manner. PDT exerts its cytotoxic effects primarily through the generation of ROS, which cause extensive damage to cellular components and lead to cell death²⁴. In this study, we used DCFDA probe to measure overall intracellular oxidative stress. DCFDA detects cumulative ROS levels, including hydrogen peroxide, hydroxyl radicals, and singlet oxygen, providing a broad and representative measure of oxidative stress. This method allowed us to compare the total ROS levels induced by ZnPc1 and ZnPc2 and to observe their correlation with cytotoxic and anti-angiogenic effects. The consistent increase in oxidative stress measured by DCFDA aligns with the observed biological effects, including cell death and anti-angiogenic activity, validating its use in our experiments. The use of DCFDA is a widely accepted approach in photodynamic therapy research for evaluating oxidative stress, especially in initial studies, without distinguishing individual ROS species^{25,26}. However, species specific detections such as scavenger-based methods could provide a deeper understanding into the underlying mechanism of ROS generation could be

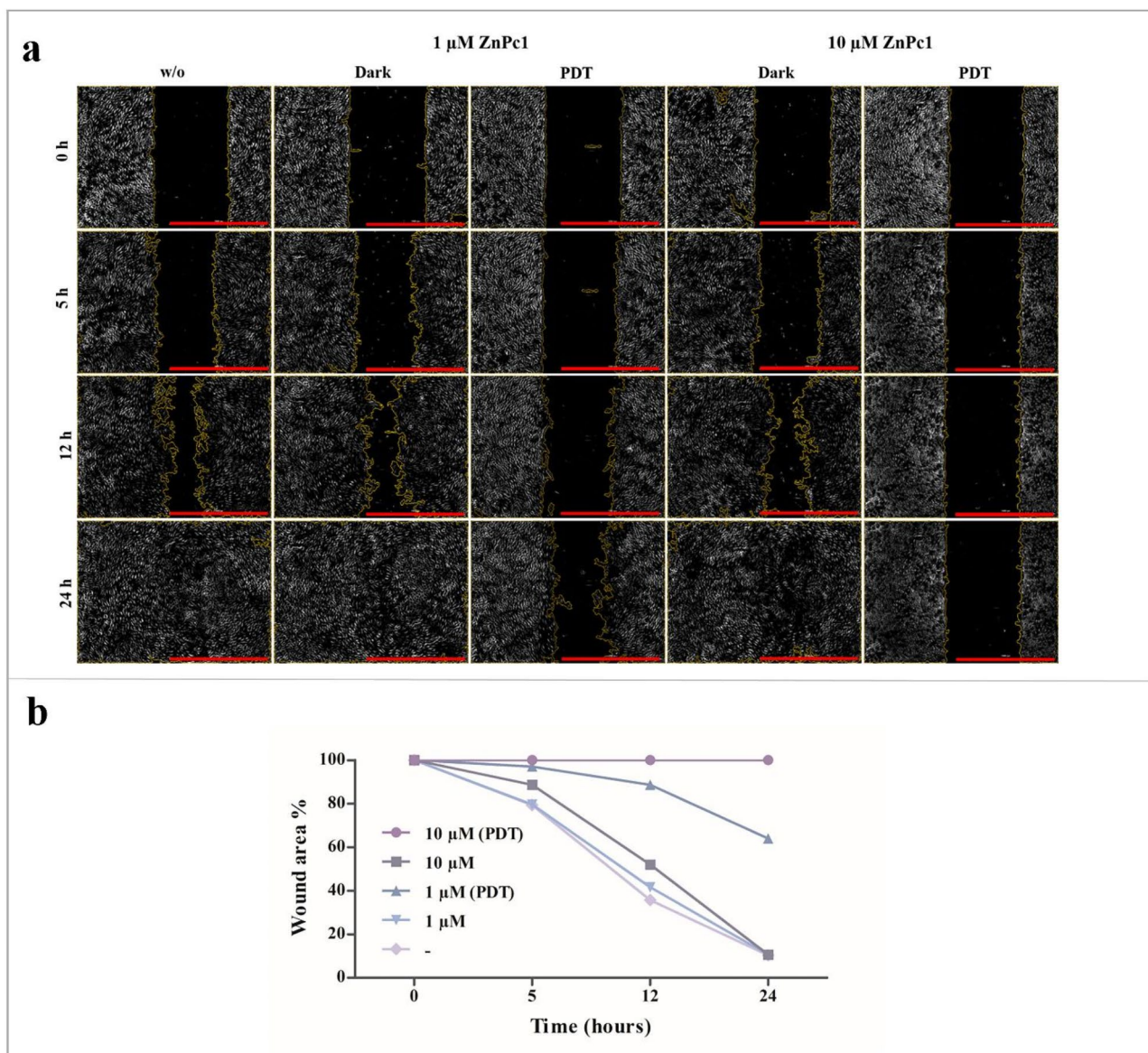


Fig. 3. The effect of ZnPc1-PDT on the spontaneous migration of HUVECs was evaluated using a wound healing assay. **(a)** Images were taken at 0, 5, 12, and 24 h, and **(b)** the wound closure was quantified. At 24 h, the wounds in the untreated cells and the dark group (w/o PDT) were completely closed. However, PDT treatment significantly inhibited the wound closure ability of HUVECs in a dose-dependent manner. Scale bar: 1 mm.

useful for further investigation. In order to better understand the underlying mechanisms, ROS formation was assessed at two key time points: 30 min (immediate) and 24 h (delayed) post-PDT. The significant elevation in ROS levels, particularly 24 h post-treatment, highlights the prolonged oxidative stress induced by PDT. Results indicated that ZnPc1 triggered a stronger cytotoxic response than ZnPc2 and was also more effective in ROS production. These findings suggest a clear correlation between cytotoxic response and ROS levels, indicating that the cytotoxic effect is closely linked to the extent of ROS generation. Numerous studies have underscored the critical role of ROS generation post-PDT in initiating oxidative damage and subsequent cell death²⁷, which is consistent with our findings. PDT initiates ROS production, which leads to cellular damage and triggers apoptosis, necrosis, or a combination of both. Similar to the cytotoxicity results, ZnPc did not induce apoptosis or necrosis in the dark. The findings suggest that apoptosis is the primary cell death mechanism induced by both ZnPc-PDT treatments, particularly at both high and low concentrations of ZnPc2 and only at low doses of ZnPc1. The observed increase in necrotic cell death, particularly at higher concentrations of ZnPc1, correlated with the extensive ROS production induced by ZnPc1-PDT. Studies have reported that, while moderate levels of ROS activate apoptosis, an energy-dependent and regulated process, excessive ROS production triggers necrosis^{28,29}, which aligns with our findings. Apoptosis requires sufficient intracellular ATP for its execution, and when ATP levels become inadequate, cells shift toward necrotic death. This transition from apoptosis to

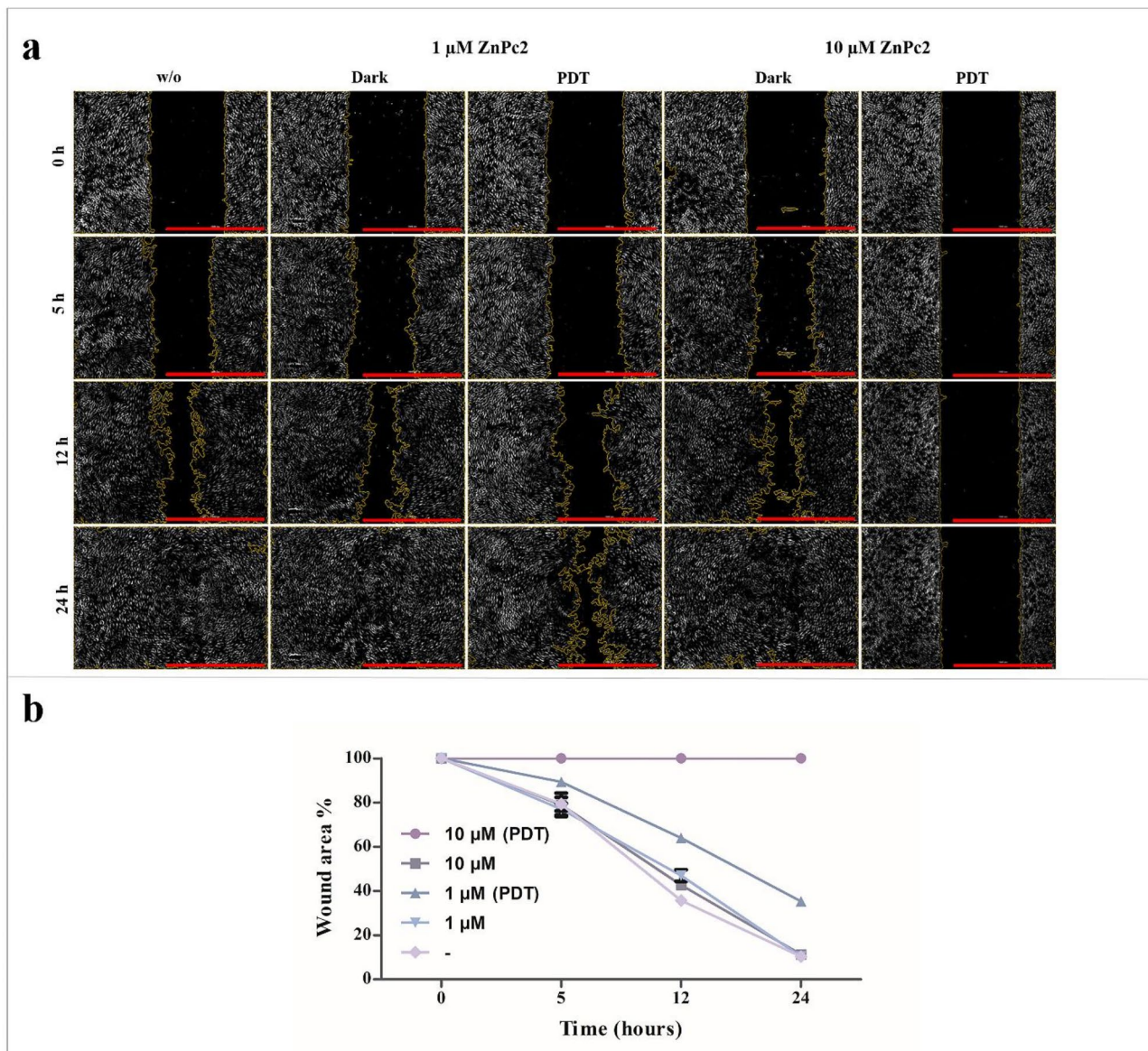


Fig. 4. The effect of ZnPc2-PDT on the spontaneous migration of HUVECs was evaluated using a wound healing assay. **(a)** Images were taken at 0, 5, 12, and 24 h, and **(b)** the wound closure was quantified. At 24 h, the wounds in the untreated cells and the dark group (w/o PDT) were completely closed. However, PDT treatment significantly inhibited the wound closure ability of HUVECs in a dose-dependent manner. Scale bar: 1 mm.

necrosis is primarily driven by ROS-induced mitochondrial dysfunction, which impairs ATP production and disrupts the energy supply required for apoptosis, making necrosis the predominant mode of cell death^{30,31}. The enhanced necrotic response observed with ZnPc1 at higher concentrations is likely due to excessive ROS generation, which overwhelms cellular repair mechanisms and leads to a shift from apoptosis to necrosis. In contrast, ZnPc2 generates moderate levels of ROS, which predominantly trigger apoptotic cell death. These differences may also arise from variations in the subcellular localization of ZnPc1 and ZnPc2, influencing the type and extent of cellular damage.

Angiogenesis is essential for tumor growth and metastasis, as tumors rely on new blood vessels to supply nutrients and oxygen. Endothelial cells respond to VEGF secreted by tumor cells under hypoxic conditions to drive angiogenesis. Endothelial cell migration and invasion are critical processes in angiogenesis and are essential for tumor growth and metastasis. Consequently, the inhibition of migration and invasion has significant implications for anti-angiogenic therapy. PDT-induced oxidative stress disrupts cytoskeletal organization, focal adhesions, and integrin-mediated cell adhesion in endothelial cells, all of which are vital processes required for migration toward angiogenic stimuli³². Studies have reported the anti-angiogenic potential of PDT by disrupting the migration and invasion of endothelial cells and impairing the formation of new blood vessels^{6,33}. In addition to their cytotoxic effects, the anti-angiogenic properties of ZnPc-PDT were evaluated on HUVECs using

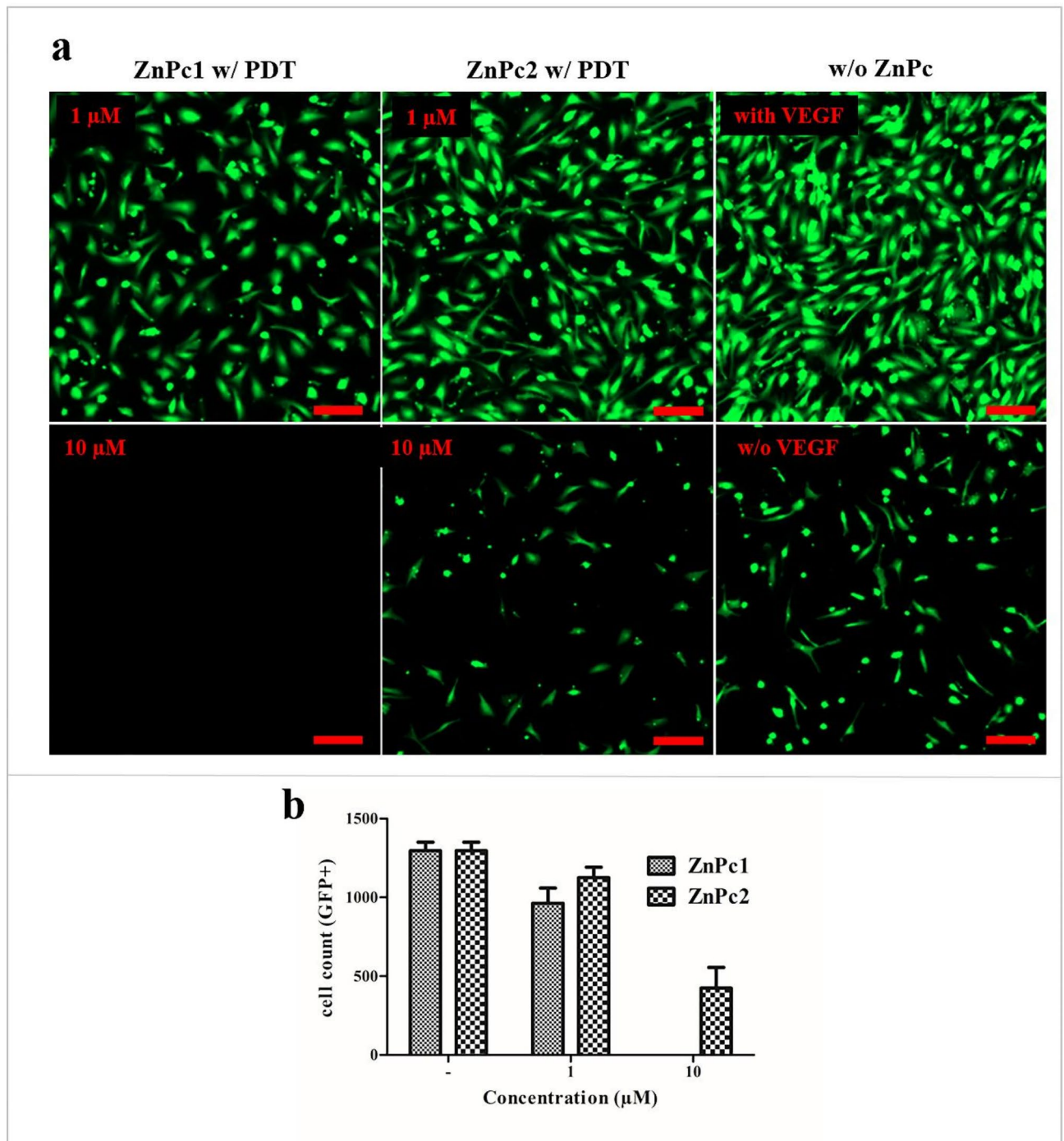


Fig. 5. The effect of ZnPc-PDT on HUVEC migration toward VEGF-containing medium was evaluated using transwell. **(a)** After 24 h post-PDT with ZnPcs, the migrated cells were stained with Calcein AM. **(b)** The number of migrated cells was quantified after 24 h. The migration of HUVECs was significantly stimulated by the presence of VEGF as a chemoattractant, while the number of migrated cells was substantially reduced in the absence of VEGF. Both ZnPcs demonstrated an inhibitory effect on migration in a dose-dependent manner, with ZnPc1 exhibiting significantly greater inhibition than ZnPc2. Notably, at higher concentrations, ZnPc1 completely blocked HUVEC migration. Results are presented as mean \pm SD ($n = 3$). Scale bar: 200 μ m.

spontaneous and directional migration and invasion assays. For migration assay there is an inherent limitation in distinguishing migration from proliferation. In order to address this, we utilized a starvation medium 18 h prior to treatment to arrest cells in the G_0 phase of the cell cycle, thereby effectively inhibiting proliferation. This approach ensures that the observed effects on migration assays are predominantly attributable to inhibited migration. The results indicated a stronger inhibitory effect of ZnPc1 on wound healing than that of ZnPc2. Furthermore, HUVEC migration and invasion toward the chemoattractant was significantly inhibited after 24 h

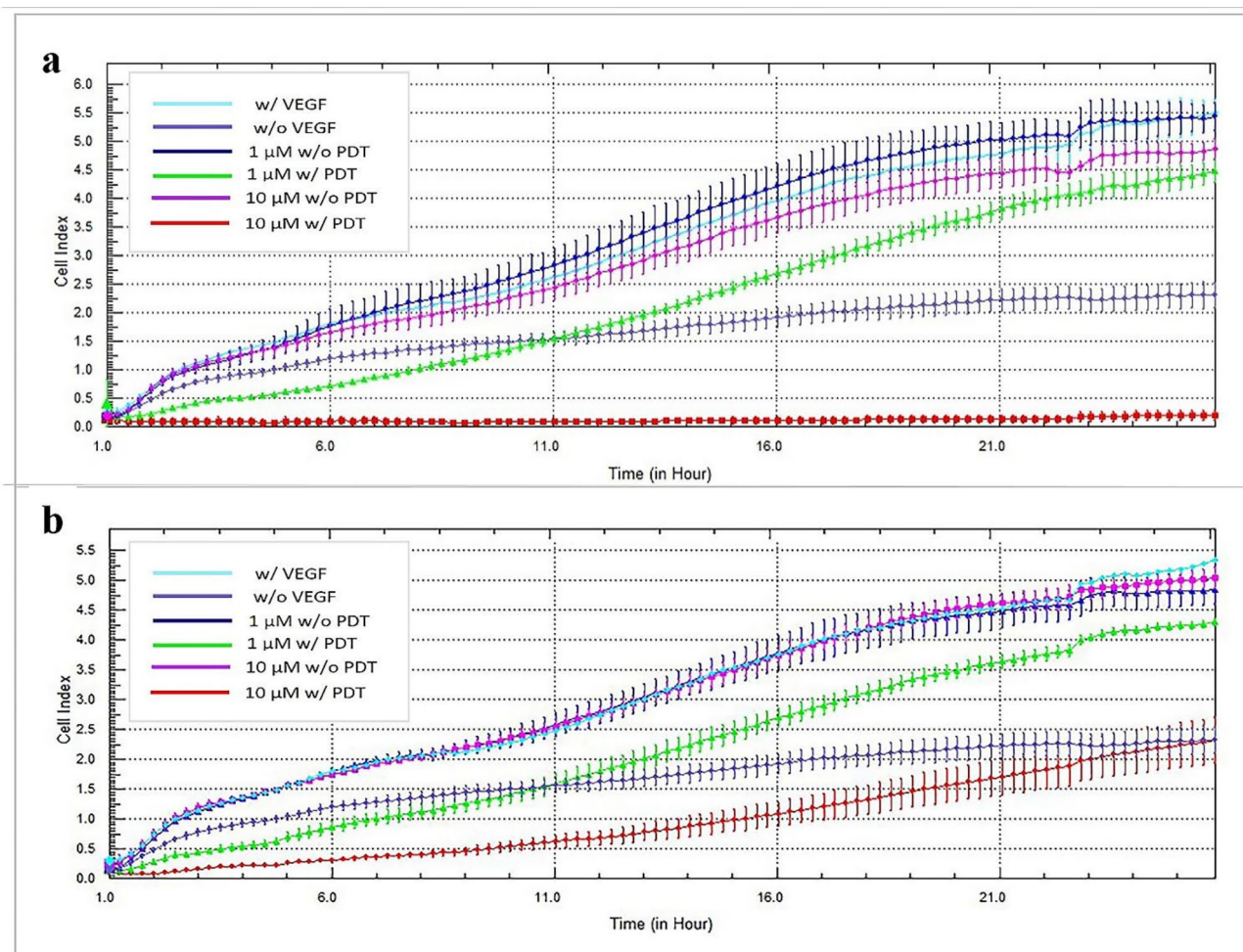


Fig. 6. Kinetic curves showing HUVEC migration following photodynamic therapy (PDT) with (a) ZnPc1 and (b) ZnPc2 were assessed using the xCELLigence RTCA-DP system. VEGF-containing media served as a chemoattractant in the lower chamber. Impedance measurements were recorded every 15 min over a 24-h period. Results are expressed as the mean \pm SD. PDT light dose: 20 joules.cm⁻²; Pc concentration range: 1–10 μ M. Color codes indicated the concentrations of the molecules: cyan (with VEGF), and slate blue (w/o VEGF), dark blue (1 μ M w/o PDT), magenta (10 μ M w/o PDT), green (1 μ M with PDT), red (10 μ M with PDT).

of PDT, particularly at high ZnPc concentrations. The inhibitory effect of ZnPc-PDT on cell invasion was more pronounced than on migration, suggesting that matrix metalloproteinase activity in the cells may be further affected by PDT. Real-time migration assay showed that continuous and sustained increases in migration were exhibited by untreated cells over time, whereas dose-dependent inhibition was induced by ZnPc1 and ZnPc2, consistent with observations from endpoint migration assays. Although ZnPc2-PDT significantly inhibited cell migration and invasion at high concentrations, ZnPc1-PDT exerted a stronger effect than ZnPc2. Findings from both the wound healing and transwell assays underscore the potent inhibitory capacity of ZnPc on HUVEC migration and invasion. In order to extend these investigations, VEGF secretion analysis could provide a valuable insight for future research to further elucidate the VEGF-related anti-angiogenic mechanisms of Pcs. Tube formation by endothelial cells is a hallmark of angiogenesis, and its inhibition likely results from both direct cytotoxic effects on endothelial cells and the disruption of key signaling pathways involved in angiogenesis^{31,33}. The findings indicated that ZnPc1 exhibits a superior inhibitory effect on tube formation, even at lower concentrations. Inhibition of endothelial cell tube formation through ZnPc1-PDT offers a promising strategy for blocking tumor angiogenesis, particularly in aggressive tumors, where angiogenesis is critical to disease progression.

Conclusion

The anti-angiogenic effects of two cationic phthalocyanines (ZnPc1 and ZnPc2), whose synthesis and characterization were carried out in accordance with the literature, were studied. Angiogenesis is a complex, multi-step process that involves endothelial cell proliferation, migration, tube formation, and matrix remodeling. ZnPc-PDT demonstrated significant cytotoxic and anti-angiogenic effects in HUVECs. These molecules exhibit a similar mechanism of action: they generate ROS upon light activation, which subsequently induces endothelial

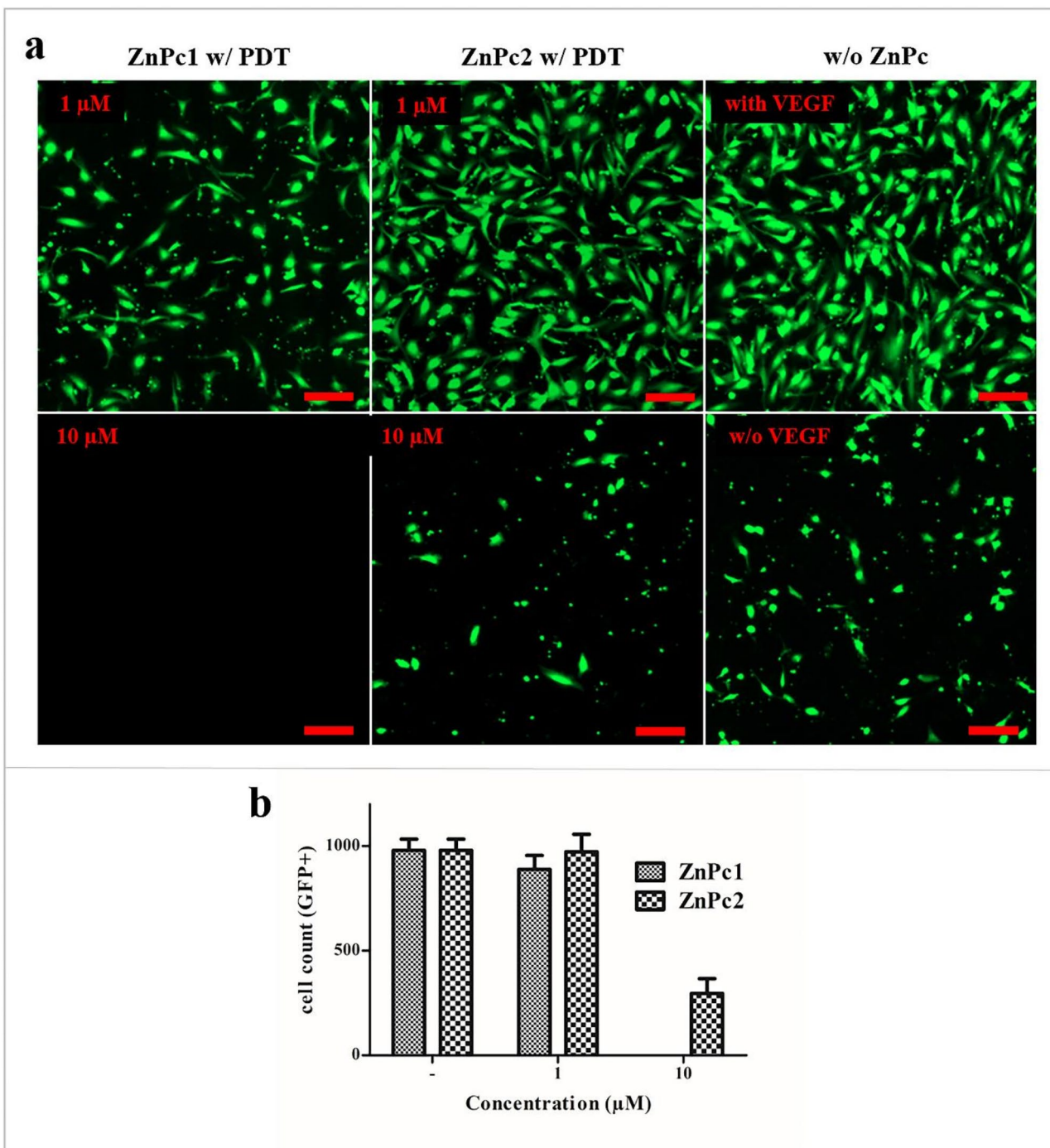


Fig. 7. The effect of ZnPc-PDT on HUVEC invasion toward VEGF-containing medium was evaluated using Matrigel-coated transwell. **(a)** After 24 h post-PDT with ZnPcs, the invaded cells were stained with Calcein AM. **(b)** The number of invaded cells was quantified after 24 h. The invasion of HUVECs was significantly stimulated by the presence of VEGF as a chemoattractant, while the number of invaded cells was substantially reduced in the absence of VEGF. Both ZnPcs demonstrated an inhibitory effect on invasion in a dose-dependent manner, with ZnPc1 exhibiting significantly greater inhibition than ZnPc2. Notably, at higher concentrations, ZnPc1 completely blocked HUVEC invasion. Results are presented as mean \pm SD. Scale bar: 200 μ m.

cell death and disrupts critical angiogenic processes. Although both molecules exhibited dose-dependent effects, notable differences in efficacy were observed. ZnPc1 produced a markedly stronger cytotoxic, anti-migratory, and anti-angiogenic effect than ZnPc2. In the absence of light, both ZnPc compounds had negligible effects on HUVECs, confirming that their inhibitory activities were highly dependent on photodynamic activation. The overall findings underscore the potential of ZnPcs, particularly ZnPc1, as potent photosensitizers in PDT to

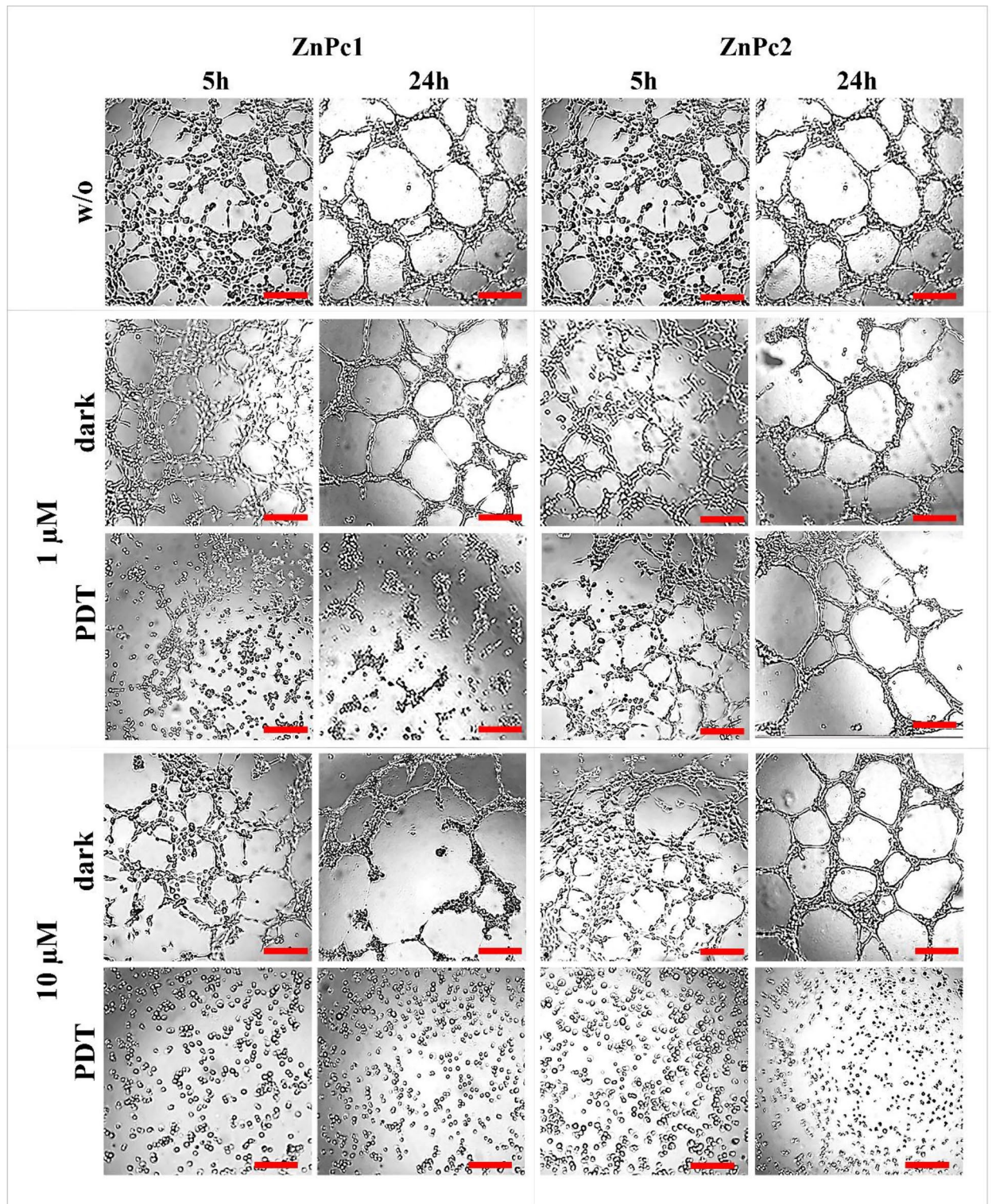


Fig. 8. The effect of ZnPc-PDT on HUVEC tube formation was assessed following treatment with ZnPcs and subsequent PDT. Tubular structures, defined as networks of cells forming junctions and elongations resembling capillary-like structures, were monitored at 5 and 24 h using phase-contrast microscopy. In the untreated control, HUVECs reorganized into tubular-like formations after 5 h, and complete lumen structures were observed by 24 h, indicating angiogenesis process. ZnPc treatment inhibited tube formation in a dose-dependent manner, with ZnPc1 exhibiting a greater inhibitory effect than ZnPc2. Even at lower concentrations, ZnPc1 significantly suppressed tube formation. Scale bar: 200 μm .

target both tumor cells and tumor-associated vasculature. By inhibiting key endothelial cell functions, including the induction of ROS-dependent apoptosis and the suppression of spontaneous and directed migration, invasion, and tube formation, ZnPc1-PDT offers a promising strategy for integrated antitumor and antiangiogenic therapy in cancer treatment.

Data availability

The data that support the findings of this study are available from the corresponding author upon reasonable request.

Received: 17 November 2024; Accepted: 25 December 2024

Published online: 20 January 2025

References

- Liu, Z. L., Chen, H. H., Zheng, L. L., Sun, L. P. & Shi, L. Angiogenic signaling pathways and anti-angiogenic therapy for cancer. *Signal. Transduct. Target. Ther.* **8**, 198. <https://doi.org/10.1038/s41392-023-01460-1> (2023).
- De Palma, M. & Hanahan, D. Milestones in tumor vascularization and its therapeutic targeting. *Nat. Cancer* **5**, 827–843. <https://doi.org/10.1038/s43018-024-00780-7> (2024).
- Jiang, W., Liang, M., Lei, Q., Li, G. & Wu, S. The current status of photodynamic therapy in cancer treatment. *Cancers* **15**, 585. <https://doi.org/10.3390/cancers15030585> (2023).
- Szafraniec, M. J., Toporkiewicz, M. & Gamian, A. Zinc-substituted pheophorbide a is a safe and efficient antivascular photodynamic agent. *Pharmaceuticals* **15**, 235. <https://doi.org/10.3390/ph15020235> (2022).
- Suzuki, T. et al. Vascular shutdown by photodynamic therapy using talaporfin sodium. *Cancers* **12**, 2369. <https://doi.org/10.3390/cancers12092369> (2020).
- Stupáková, V. et al. Photodynamic effect of hypericin in primary cultures of human umbilical endothelial cells and glioma cell lines. *Phytother. Res.* **23**, 827–832. <https://doi.org/10.1002/ptr.2681> (2009).
- Xue, J., Gruber, F., Tschachler, E. & Zhao, Y. Crosstalk between oxidative stress, autophagy and apoptosis in hemoporphin photodynamic therapy treated human umbilical vein endothelial cells. *Photodiagn. Photodyn. Ther.* **33**, 102137. <https://doi.org/10.1016/j.pdpdt.2020.102137> (2021).
- Chen, D. et al. A highly-efficient type I photosensitizer with robust vascular-disruption activity for hypoxic-and-metastatic tumor specific photodynamic therapy. *Small* **16**, 2001059. <https://doi.org/10.1002/sml.202001059> (2020).
- Hattori, S. et al. Photodynamic effect of amphiphilic N \wedge C \wedge N-Coordinated platinum (II) complexes in human umbilical vein endothelial cells. *Inorg. Chem.* **63**, 13972–13979. <https://doi.org/10.1021/acs.inorgchem.4c01414> (2024).
- Nesterova, I. V. et al. Metallo-phthalocyanine near-IR fluorophores: Oligonucleotide conjugates and their applications in PCR assays. *Bioconjug. Chem.* **18**, 2159–2168. <https://doi.org/10.1021/bc700233w> (2007).
- Taquet, J. P., Frochet, C., Manneville, V. & Barberi-Heyob, M. Phthalocyanines covalently bound to biomolecules for a targeted photodynamic therapy. *Curr. Med. Chem.* **14**, 1673–1687. <https://doi.org/10.2174/092986707780830970> (2007).
- Li, D. et al. Innovative design strategies advance biomedical applications of phthalocyanines. *Adv. Healthc. Mater.* **12**, 2300263. <https://doi.org/10.1002/adhm.202300263> (2023).
- Ma, C. et al. Caspase-1 regulates the apoptosis and pyroptosis induced by phthalocyanine zinc-mediated photodynamic therapy in breast cancer MCF-7 cells. *Molecules* **28**, 5934. <https://doi.org/10.3390/molecules28165934> (2023).
- Valli, F., Vior, M. C. G., Roguin, L. P. & Marino, J. Crosstalk between oxidative stress-induced apoptotic and autophagic signaling pathways in Zn (II) phthalocyanine photodynamic therapy of melanoma. *Free Radic Biol. Med.* **152**, 743–754. <https://doi.org/10.1016/j.freeradbiomed.2020.01.018> (2020).
- Akkoç, B. et al. Pegylated metal-free and zinc (II) phthalocyanines: synthesis, photophysical/chemical properties and in vitro photodynamic activities against head, neck and colon cancer cell lines. *Dalton Trans.* **51**, 10136–10147. <https://doi.org/10.1039/D2DT00704E> (2022).
- Schmidt, J. et al. Novel zinc- and silicon-phthalocyanines as photosensitizers for photodynamic therapy of cholangiocarcinoma. *Int. J. Mol. Med.* **42**, 534–546. <https://doi.org/10.3892/ijmm.2018.3620> (2018).
- Kuzyniak, W. et al. Tetra-triethylenesulfonated zinc phthalocyanine for photodynamic cancer therapy. *Photodiagn. Photodyn. Ther.* **13**, 148–157. <https://doi.org/10.1016/j.pdpdt.2015.07.001> (2016).
- Lv, F., Cao, B., Cui, Y. & Liu, T. Zinc phthalocyanine labelled polyethylene glycol: Preparation, characterization, interaction with bovine serum albumin and near infrared fluorescence imaging in vivo. *Molecules* **17**, 6348–6361. <https://doi.org/10.3390/molecules17066348> (2012).
- Marino, J., Vior, M. C. G., Dicalio, L. E., Roguin, L. P. & Awruch, J. Photodynamic effects of isosteric water-soluble phthalocyanines on human nasopharynx KB carcinoma cells. *Eur. J. Med. Chem.* **45**, 4129–4139. <https://doi.org/10.1016/j.ejmech.2010.06.002> (2010).
- Bird, C. & Kirstein, S. Real-time, label-free monitoring of cellular invasion and migration with the xCELLigence system. *Nat. Methods* **6**. <https://doi.org/10.1038/nmeth.f.263> (2009).
- Justus, C. R., Marie, M. A., Sanderlin, E. J. & Yang, L. V. Transwell in vitro cell migration and invasion assays. *Cell. Viability Assays* 349–359. https://doi.org/10.1007/978-1-0716-3052-5_22 (2023).
- Arnautova, I. & Kleinman, H. K. In vitro angiogenesis: Endothelial cell tube formation on gelled basement membrane extract. *Nat. Protoc.* **5**, 628–635. <https://doi.org/10.1038/nprot.2010.6> (2010).
- Wöhrl, D. et al. Synthesis of positively charged phthalocyanines and their activity in the photodynamic therapy of cancer cells. *Photochem. Photobiol.* **51**, 351–356. <https://doi.org/10.1111/j.1751-1097.1990.tb01721.x> (1990).
- Dąbrowski, J. M. Reactive oxygen species in photodynamic therapy: Mechanisms of their generation and potentiation. *Adv. Inorg. Chem.* **70**, 343–394. <https://doi.org/10.1016/bs.adioch.2017.03.002> (2017).
- Wang, S. et al. Photodynamic-chemodynamic cascade reactions for efficient drug delivery and enhanced combination therapy. *Adv. Sci.* **8**(10), 2002927. <https://doi.org/10.1002/advs.202002927> (2021).
- Monroe, J. D., Belekov, E., Er, A. O. & Smith, M. E. Anticancer photodynamic therapy properties of sulfur-doped graphene quantum dot and methylene blue preparations in MCF-7 breast cancer cell culture. *Photochem. Photobiol.* **95**(6), 1473–1481. <https://doi.org/10.1111/php.13136> (2019).
- Thannickal, V. J. & Fanburg, B. L. Reactive oxygen species in cell signaling. *Am. J. Physiol. Lung Cell. Mol. Physiol.* **279**. <https://doi.org/10.1152/ajplung.2000.279.6.L1005> (2000).
- Chandra, J., Samali, A. & Orrenius, S. Triggering and modulation of apoptosis by oxidative stress. *Free Radic Biol. Med.* **29**, 323–333. [https://doi.org/10.1016/S0891-5849\(00\)00302-6](https://doi.org/10.1016/S0891-5849(00)00302-6) (2000).
- Alexandre, J. et al. Accumulation of hydrogen peroxide is an early and crucial step for paclitaxel-induced cancer cell death both in vitro and in vivo. *Int. J. Cancer* **119**, 41–48. <https://doi.org/10.1002/ijc.21685> (2006).
- He, Y. et al. Integrated transcriptome analysis reveals the impact of photodynamic therapy on cerebrovascular endothelial cells. *Front. Oncol.* **11**, 731414. <https://doi.org/10.3389/fonc.2021.731414> (2021).

31. Wang, W., Moriyama, L. T. & Bagnato, V. S. Photodynamic therapy induced vascular damage: An overview of experimental PDT. *Laser Phys. Lett.* **10**(2), 023001. <https://doi.org/10.1088/1612-2011/10/2/023001> (2012).
32. Pathak, A., Pal, A. K., Roy, S., Nandave, M. & Jain, K. Role of angiogenesis and its biomarkers in development of targeted tumor therapies. *Stem Cells Int* 9077926. <https://doi.org/10.1155/2024/9077926> (2024).
33. Lopes-Coelho, F., Martins, F., Pereira, S. A. & Serpa, J. Anti-angiogenic therapy: Current challenges and future perspectives. *Int. J. Mol. Sci.* **22**, 3765. <https://doi.org/10.3390/ijms22073765> (2021).

Acknowledgements

This study was supported by the Scientific and Technological Research Council of Turkey (TUBITAK) under Grant Number 216S387. The authors thank TUBITAK for their support.

Author contributions

S.I. and M.S. designed the concept and cellular-based experiments and analyzed the data. S.I. performed the experiments. E.H., M.O., and A.K.B. provided Pc molecules. M.S. and O.C. supervised the study. S.I. wrote the main manuscript text and prepared figures. The manuscript was written with the contributions of all authors. All authors approved the final version of the manuscript.

Declarations

Competing interests

The authors declare no competing interests.

Additional information

Supplementary Information The online version contains supplementary material available at <https://doi.org/10.1038/s41598-024-84674-9>.

Correspondence and requests for materials should be addressed to O.C. or M.S.

Reprints and permissions information is available at www.nature.com/reprints.

Publisher's note Springer Nature remains neutral with regard to jurisdictional claims in published maps and institutional affiliations.

Open Access This article is licensed under a Creative Commons Attribution-NonCommercial-NoDerivatives 4.0 International License, which permits any non-commercial use, sharing, distribution and reproduction in any medium or format, as long as you give appropriate credit to the original author(s) and the source, provide a link to the Creative Commons licence, and indicate if you modified the licensed material. You do not have permission under this licence to share adapted material derived from this article or parts of it. The images or other third party material in this article are included in the article's Creative Commons licence, unless indicated otherwise in a credit line to the material. If material is not included in the article's Creative Commons licence and your intended use is not permitted by statutory regulation or exceeds the permitted use, you will need to obtain permission directly from the copyright holder. To view a copy of this licence, visit <http://creativecommons.org/licenses/by-nc-nd/4.0/>.

© The Author(s) 2025